Inorganic Chemistry

Article

pubs.acs.org/IC

Syntheses, Crystal Structures, Ion-Exchange, and Photocatalytic Properties of Two Amine-Directed Ge−Sb−S Compounds

Bo Zhang,[†,‡] Mei-Ling Feng,[†] Hong-Hua Cui,[†] Cheng-Feng Du,[†,‡] Xing-Hui Qi,[†,§] Nan-Nan Shen,[†,‡] and Xiao-Ying Huang*[,†]

[†]State Key Laboratory of Structural Chemistry, Fujian Institute of Research on the Structure of Matter, Chinese Academy of Sciences, Fuzhou, Fujian 350002, P. R. China

[‡]University of Chinese Academy of Sciences, Beijing, 100049, P. R. China

[§]College of Chemistry, Fuzhou University, Fuzhou, Fujian 350002, P. R. China

Supporting Information

ABSTRACT: Among numerous heterometallic chalcogenidoantimonates, relatively a few amine-directed Ge−Sb−S compounds have been synthesized. Presented here are the solvothermal syntheses, crystal structures, and ion-exchange, optical, and photocatalytic properties of two novel amine-directed Ge−Sb−S compounds, namely, $[CH_3NH_3]_{20}Ge_{10}Sb_{28}S_{72}\cdot 7H_2O$ (**1**) and $[(CH_3CH_2CH_2)_2NH_2]_3Ge_3Sb_5S_{15}\cdot 0.5(C_2H_5OH)$ (**2**). The structure of **1** features an unprecedented two-dimensional Ge−Sb−S double-layer composed of two twofold rotational symmetry-related thick $[Ge_8Sb_{28}S_{72}]_n^{28n-}$ single layers adhered via vertex-sharing $[GeS_4]$ tetrahedra. Compound **2** features a unique $[Ge_3Sb_5S_{15}]_n^{3n-}$ slab perforated with large elliptic-like windows. Remarkably, compound **1** exhibited excellent Cs^+ ion-exchange property despite the presence of excess competitive cations, such as Na^+, K^+, Mg^{2+}, and Ca^{2+} ions. In addition, compound **1** displayed visible-light-driven photocatalytic activity for degradation of rhodamine B.

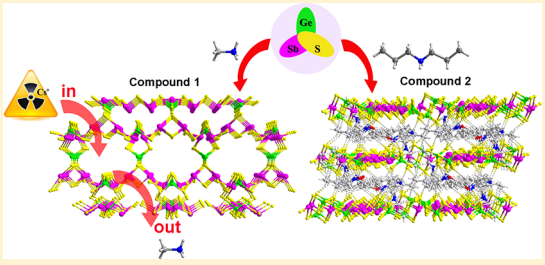

INTRODUCTION

Chalcogenidometalates are of continuous interest due to their fascinating structures and potential applications in the fields of ion-exchange,[1] photocatalysis,[2] ion conductivity,[3] thermoelectrics,[4] and so on.[5] Recently, much effort has been devoted to the synthesis of heterometallic chalcogenidometalates based on the Sb(III) ion that is characteristic of its non-centrosymmetrical coordination geometry caused by the lone-pair electrons and its pronounced tendency of forming various condensed polyanions.[1d−f] Indeed, the combination of Sb(III) and a second metal ion (typically tetrahedral metal ion) has resulted in numerous heterometallic chalcogenidometalates with great structural and compositional diversities, as well as interesting properties.[1e,6] Among them, the M−Sb−Q compounds (M = Hg^{2+}, Ag^+, Cu^+, Mn^{2+}, Ga^{3+}, and In^{3+}; Q = S^{2-}, Se^{2-}) have been well-documented.[6d−f,7] By contrast, the Ge−Sb−S compounds are rarely explored. The limited examples include zero-dimensional (0D), one-dimensional (1D), two-dimensional (2D), and three-dimensional (3D) compounds 0D-$[(Me)_2NH_2]_6[(Ge_2Sb_2S_7)(Ge_4S_{10})]$,[6c] 1D-$[AEPH_2][GeSb_2S_6]\cdot CH_3OH$ (AEP = *N*-(2-aminoethyl)-piperazine),[6i] 1D-$[(Me)_2NH_2][DabcoH]_2[Ge_2Sb_3S_{10}]$ (Dabco = triethylenediamine),[6c] 2D-$[M(en)_3][GeSb_2S_6]$ (M = Mn, Co, Ni, Ge; en = ethylenediamine),[6c,8] 2D-$[Co(dien)_2]_2GeSb_4S_{10}$ (dien = diethylenetriamine),[8a] 2D-$[Ni(dien)_2]_3[Ge_3Sb_8S_{21}]\cdot 0.5H_2O$[9] and 3D-$[(Me)_2NH_2]_2[GeSb_2S_6]$.[1f]

Organic amines have been widely used in the solvothermal synthesis of chalcogenidometalates owing to their structure-directing effects. More importantly, the introduction of organic amines may engender interesting properties. For instance, the amine-directed M−Sb−S compounds such as 2D-$[(Me)_2NH_2]_2[Ga_2Sb_2S_7]\cdot H_2O$,[1e] 3D-$[CH_3NH_3]_4[In_4SbS_9SH]$,[1d] 2D-$[(CH_3CH_2CH_2)_2NH_2]_5In_5Sb_6S_{19}\cdot 1.45H_2O$[6h] and 3D-$[(Me)_2NH_2]_2[GeSb_2S_6]$[1f] exhibit excellent ion-exchange properties. In particular, the $[(Me)_2NH_2]_2[GeSb_2S_6]$ represents the first 3D chiral microporous Ge−Sb−S compound with high ion-exchange capacity and high selectivity for Cs^+ ion. Herein, we report the syntheses, crystal structures, and properties of two amine-directed layered Ge−Sb−S compounds, namely, $[CH_3NH_3]_{20}Ge_{10}Sb_{28}S_{72}\cdot 7H_2O$ (**1**) and $[(CH_3CH_2CH_2)_2NH_2]_3Ge_3Sb_5S_{15}\cdot 0.5(C_2H_5OH)$ (**2**). Compound **1** features an unusual double-layered structure, while **2** features a unique $[Ge_3Sb_5S_{15}]_n^{3n-}$ layer with large elliptic-like windows. Remarkably, compound **1** showed outstanding cation-exchange properties with the specificity for Cs^+ ion against other cations of lower softness such as Na^+, K^+, Mg^{2+}, and Ca^{2+} ions. Additionally, compound **1** displayed visible-light-driven photocatalytic activity for degradation of rhodamine B.

Received: May 25, 2015
Published: August 20, 2015

ACS Publications © 2015 American Chemical Society

DOI: 10.1021/acs.inorgchem.5b01181
Inorg. Chem. 2015, 54, 8474−8481

EXPERIMENT SECTION

Materials and Methods. GeO_2 and S (99.99%) were purchased from Xin Long Te Technology Development Co., Ltd. (Sichuan, China); methylammonium (33−40% alcohol solution) was purchased from Aladdin Company (Shanghai, China). Other reagents were of analytical grade and purchased from Sinopharm Chemical Reagent Co., Ltd. (Shanghai, China). All the chemicals were used without further purification.

Elemental analyses (EA) of C, H, and N were performed using a German Elementary Vario EL III instrument. Energy-dispersive spectroscopy (EDS) was recorded on a JEOL JSM-6700F scanning electron microscope. The solid-state ultraviolet−visible (UV−vis) spectra were measured at room temperature using a UV−vis−NIR Varian 86 Cary 500 Scan spectrophotometer for compound **1** and Cs^+-exchanged product of compound **1** and a Shimadzu UV-2600 spectrophotometer for compound **2**. A $BaSO_4$ plate was used as a standard (100% reflectance). The absorption spectra were calculated from diffuse reflectance spectra by using the Kubelka−Munk function: $a/S = (1 - R)^2/2R$, where a is the absorption coefficient, S is the scattering coefficient, which is practically independent of wavelength when the particle size is larger than 5 μm, and R is the reflectance.[10a] For a crystalline semiconductor with a direct band gap, its optical absorption near the band edge follows the equation given by Tauc, $(\alpha E)^2 = A(E - E_g)$, where α is the absorption coefficient, A is the proportionality constant, E is the photon energy, and E_g is the optical band gap.[10b] Fourier transform infrared (FT-IR) spectra were taken on a Nicolet Magna 750 FT-IR spectrometer in the 4000−400 cm^{-1} region by using KBr pellets. Thermogravimetric analyses (TGA) were performed with a Netzsch STA449C at a heating rate of 5 °C/min under a nitrogen atmosphere. Powder X-ray diffraction (PXRD) patterns were collected at room temperature on a Miniflex II diffractometer using Cu Kα radiation (λ = 1.5406 Å) in the 2θ range of 5−65°. Atomic absorption spectroscopy (AAS) was performed on a ContrAA 700. The supernate of photocatalytic experiment was analyzed with the help of UV−vis absorption spectra instrument (PerkinElmer Lambda 350 UV−vis spectrometer).

Synthesis of Compound 1. A mixture of 0.105 g of GeO_2 (1 mmol), 0.341 g of Sb (2.8 mmol), 0.272 g of S (8.5 mmol), and 4 mL methylammonium (33−40% alcohol solution) was sealed in a 23 mL Teflon-lined stainless steel autoclave, which was heated at 160 °C for 7 d and then cooled to room temperature naturally. The products were isolated in air by filtration and washed with deionized water and ethanol, respectively, giving rise to yellow platelike crystals (46% yield based on GeO_2). It is emphasized that the crystallization of compound **1** is sensitive to the reaction temperature and time, cooling rate, and the dosage of structural directing agents (SDAs). The lower temperature, shorter reaction time, and lengthy cooling time were all unfavorable conditions, and the final product was unidentified amorphous brown powders when the temperature was higher than 180 °C. However, a similar reaction by replacing an alcohol solution of methylammonium (30%−40 wt %) with aqueous methylammonium (30%−40 wt %) yielded a mixture of unidentified dark red and yellow powders only, indicating the key role of polarity of the solvent on the formation of the final product. EDS analysis gave the average Ge/Sb/S ratio of 1.0:2.5:7.5, very close to that determined by the single-crystal diffraction. Anal. Calcd (%) for $[CH_3NH_3]_{20}Ge_{10}Sb_{28}S_{72}\cdot 7H_2O$: C 3.33, H 1.87, N 3.88%; found: C 3.55, H 1.94, N 3.82%.

Synthesis of Compound 2. A mixture of GeO_2 (0.105 g, 1 mmol), Sb (0.242 g, 2 mmol), and S (0.192 g, 6 mmol) in dipropylamine/C_2H_5OH (2 mL/2 mL) was sealed in a 23 mL Teflon-lined stainless steel autoclave at 180 °C for 7 d, then cooled to room temperature. Yellow sheetlike crystals of compound **2** (manually selected, yield: 0.040 g, 7.35% based on GeO_2) were obtained. The products were isolated in air by filtration and washed with deionized water and ethanol, respectively. EDS analysis gave the average Ge/Sb/S ratio of 1.0:1.9:4.8, very close to that determined by the single-crystal diffraction. Anal. Calcd (%) for $[(CH_3CH_2CH_2)_2NH_2]_3Ge_3Sb_5S_{15}\cdot 0.5(C_2H_5OH)$: C 13.93, H 3.13, N 2.57%; found: C 13.08, H 3.01, N 2.60%.

X-ray Crystallography. Intensity data collections of compounds **1** and **2** were performed on an Xcalibur E Oxford diffractometer with graphite-monochromated Mo Kα radiation (λ = 0.710 73 Å) at 293 K and a SuperNova Oxford diffractometer with graphite-monochromated Cu Kα radiation (λ = 1.541 84 Å) at 100 K, respectively. The structures of **1** and **2** were solved by direct methods and refined by full-matrix least-squares on F^2 using the SHELX-97 program package.[11] Non-hydrogen atoms were refined with anisotropic displacement parameters, and the hydrogen atoms attached to the C, N, and O atoms were located at geometrically calculated positions. For compound **1**, some constraints (DFIX, SIMU, and ISOR) were applied to the $[CH_3NH_3]^+$ cations to obtain the chemical−reasonable models and reasonable atomic displacement parameters. The SQUEEZE option of PLATON[12] was used in refining the structure of **1** to eliminate the contribution of disordered H_2O molecules to the reflection intensities. The B-level alerts in the checkCIF report of **1** originate from the slight disorder of some of the Sb ions (Sb(12), Sb(18), Sb(24), and Sb(28)). We ever attempted to split these Sb ions into two parts. However, the refined site occupancy factors (SOFs) of the disordered Sb ions for one of the parts were very small, and many additional soft restraints were needed. Therefore, finally we chose not to deal with such a slight disorder. In compound **2**, some constraints (DFIX, SIMU, SADI, and ISOR) were applied to the $[(CH_3CH_2CH_2)_2NH_2]^+$ cations to obtain the chemical−reasonable models and reasonable atomic displacement parameters. The empirical formulas were confirmed by the TGA and EA results. Detailed crystallographic data and structure-refinement parameters of compounds **1** and **2** are summarized in Table 1.

Table 1. Crystallographic Data for Compounds 1 and 2

	1	2
empirical formula	$C_{20}H_{134}Ge_{10}N_{20}O_7S_{72}Sb_{28}$	$C_{19}H_{51}Ge_3N_3O_{0.5}S_{15}Sb_5$
formula weight	7210.69	1637.04
crystal system	monoclinic	triclinic
space group	$C2/c$	$P\bar{1}$
a, Å	29.2964(8)	9.7628(3)
b, Å	29.3261(5)	15.7590(4)
c, Å	41.6006(10)	17.0313(4)
α, deg	90.00	79.868(2)
β, deg	100.084(2)	75.010(2)
γ, deg	90.00	81.094(2)
V, Å^3	35189.0(14)	2475.16(11)
Z	8	2
λ	0.710 73	1.541 84
T, K	293(2)	100(2)
ρ_{calcd}, g cm^{-3}	2.722	2.197
μ, mm^{-1}	6.784	29.415
$F(000)$	26 800	1562
independent refls	31 028	9868
no. of parameters	1425	524
R_1[a] ($I > 2\sigma(I)$)	0.0905	0.0299
$wR(F_2)$[b] ($I > 2\sigma(I)$)	0.1885	0.0746

[a] $R_1 = \sum||F_0| - |F_c||/\sum|F_0|$. [b] $wR_2 = [\sum w(F_0^2 - F_c^2)^2/\sum w(F_0^2)^2]^{1/2}$.

Ion-Exchange Experiments. In all the ion-exchange experiments, the solutions were prepared by adding the ground polycrystalline powders of compound **1** (0.0025 mmol, 18.0 mg) to an aqueous solution of CsCl (18 mL), corresponding to a V/m of 1000 mL/g. The mixture was kept under magnetic stirring for a period of time (e.g., 12 h) at ∼65 °C via water bath, after which the polycrystalline powder was separated by centrifugation at a speed of 9000 rpm/min for 2 min and washed several times with deionized water and ethanol. The choice of temperature of ∼65 °C was referred to the literature.[1b] The concentrations of Cs^+ in the clear supernatant were determined by AAS.

DOI: 10.1021/acs.inorgchem.5b01181
Inorg. Chem. 2015, 54, 8474−8481

Kinetics and isotherm experiments: In the kinetics experiments, the samples (~10 mL) were taken out at different time periods of ion-exchange (2, 5, 15, 30, 60, 120, 180, 720 min) from the Cs^+ solution ($C_0 \approx 150$ ppm) and processed. In the isotherm experiments, the solutions of Cs^+ with different concentrations were prepared. The ion-exchange processes lasted ~720 min, after which the samples (~10 mL) were taken out and processed.

Competitive ion-exchange experiments: The solutions with the coexistence of dilute Cs^+ ions ($C_0 \approx 9$ ppm) and individual Na^+ (187 ppm), K^+ (151 ppm), Mg^{2+} (144 ppm), and Ca^{2+} (193 ppm) were prepared, respectively, while the aqueous solution with ~123 ppm of Na^+, 2 ppm of Mg^{2+}, 6 ppm of K^+, 84 ppm of Ca^{2+}, and 2 ppm of Cs^+ ions was used to simulate Cs^+-contaminated neutral groundwater. Such solution with adjusted pH of ~10 was used to simulate typical alkaline groundwater contaminated with Cs^+ ions. The solution with the coexistence of 5 mol/L Na^+ and dilute Cs^+ ions ($C_0 \approx 9$ ppm) was used as simulated nuclear waste. Then the typical ion-exchange experiments were performed.

The pH-dependent experiments: The solutions of Cs^+ with different pH were prepared. The initial concentration of Cs^+ ion was ~9 ppm. The pH was regulated by NaOH or HCl. The ion-exchange lasted ~720 min. Subsequently, the samples were taken out and processed.

Photocatalytic Activity for Degradation of Rhodamine B. Reactions were performed in a quartz reaction vessel by mixing the photocatalyst (50 mg) with the rhodamine B aqueous solution (90 mL, 1.0×10^{-5} M) at ambient temperature. A 300 W Xe lamp equipped with a cutoff filter ($\lambda > 420$ nm) was used as the optical system. The distance between the Xe lamp and the reaction solution was ~17 cm. Prior to visible light irradiation, the dispersion was initially magnetically stirred in a dark condition for 30 min to establish an adsorption/desorption equilibrium condition. The suspension was sampled at fixed interval of 15 min. After 2 h of photoreaction, the suspension was centrifugalized at a speed of 9000 rpm/min for 2 min, and the supernate was analyzed with the help of UV−vis absorption spectra instrument (PerkinElmer Lambda 350 UV−vis spectrometer) to evaluate the capability of mineralization of rhodamine B. Meanwhile, a blank experiment in the absence of the photocatalyst under visible light irradiation was also performed, and the corresponding rhodamine B aqueous solution was dealt with via the above-mentioned method.

RESULTS AND DISCUSSION

Crystal Structure Description for Compound 1. Single-crystal X-ray diffraction analysis reveals that compound **1** crystallizes in the centrosymmetric space group $C2/c$. Its structure features an unprecedented anionic double-layered network of $[Ge_{10}Sb_{28}S_{72}]_n^{20n-}$, wherein the layers stack in an AB sequence along the c axis (Figure 1a). The asymmetric unit of compound **1** contains nine and two halves crystallographically independent Ge^{4+} ions (the Ge(1) and Ge(2) are located in 4e site with 2 symmetry), 28 Sb^{3+} ions, 72 S^{2-} ions, 20 $CH_3NH_3^+$ cations, and seven water molecules. All the Ge^{4+} ions are tetrahedrally coordinated to four S atoms with Ge−S bond distances in the range of 2.177(6)−2.229(6) Å, Figure S1a. The Sb^{3+} ions adopt three different types of coordination modes, Figure S1b−d. The first type adopts a ψ-$\{SbS_4\}$ trigonal-bipyramidal coordination geometry with three short and one long Sb−S distances (e.g., Sb(1)−S 2.455(6), 2.458(6), 2.627(7), 2.904(7) Å). The second type also adopts a ψ-$\{SbS_4\}$ trigonal-bipyramidal coordination geometry but with two short and two long Sb−S distances, respectively, in which the two long Sb−S bonds are nearly trans to each other; the fifth coordination site is occupied by the lone pairs of the Sb(III) (e.g., Sb(12)−S 2.327(6), 2.501(6), 2.858(7), 2.874(7) Å), while the third one adopts a ψ-$\{SbS_3\}$ trigonal-pyramidal coordination geometry (e.g., Sb(11)−-S 2.372(6), 2.449(7), 2.548(6) Å). Different types of coordination modes of Sb^{3+} along with the Ge^{4+} are classified in Table S1. The coordination modes of S^{2-} to Ge^{4+} and Sb^{3+} are common, and their bond lengths are in accordance with those of reported structures.[11,6c,i,8,9]

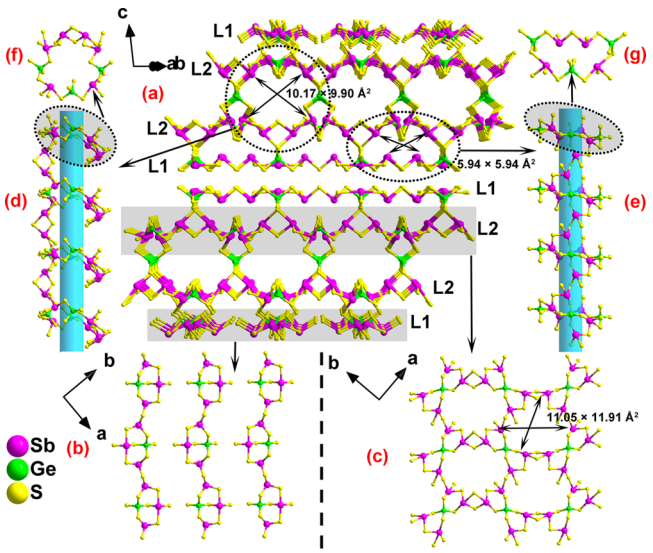

Figure 1. (a) The structure of compound **1** viewed along the [1 −1 0] direction, featuring an anionic double-layered network; (b) The L1 fraction in **1** composed of an array of chains extending along the [1 −1 0] or [1 1 0] directions; (c) the L2 layer in **1** extending along the *ab* plane; (d) the channel along the [1 −1 0] or [1 1 0] directions formed by the 18-membered froglike rings (f) interconnected by the $[Sb_2S_5]$ dimers; (e) the channel along the [1 −1 0] or [1 1 0] directions formed by 14-membered crownlike rings (g) interlinked by the $[Sb_2S_7]$ dimers. C, N, O, and H atoms were omitted for clarity.

Concisely, the anionic double-layer of compound **1** is formed by the combination of two symmetrically related (twofold rotational axis parallel to the b axis) thick single layers that are joined by Ge^{4+} ions. The thick single-layer consists of two parts denoted as L1 and L2, respectively, (Figure 1a). As illustrated in Figure 1b, the L1 is composed of arrays of 1D $[GeSb_3S_8]_n^{3n-}$ chains that are constructed by interconnecting tetranuclear $[GeSb_3S_9]$ units via corner-sharing a S^{2-} ion along the [1 −1 0] or [1 1 0] directions, while the L2 is a $[GeSb_4S_{11}]_n^{6n-}$ layer, extending along the *ab* plane, which is composed of wavelike $[Sb_4S_{11}]_n^{10n-}$ interconnected by Ge^{4+} ions, Figure 1c and S2. It is interesting that there are 20-membered $\{Ge_2Sb_8S_{10}\}$ rings in L2 formed by two $[GeS_4]$ tetrahedra and eight $[SbS_4]$ trigonal bipyramids with a rough square cross-section of 11.05 × 11.91 Å^2. It is noteworthy that all the Sb^{3+} ions in L2 adopt ψ-$\{SbS_4\}$ trigonal bipyramidal coordination geometries, whereas there are two types of coordination geometries for Sb^{3+} ions in L1, that is, $[SbS_3]$ and ψ-$[SbS_4]$. Integrally, vertex-sharing a μ_3-S^{2-} by the $[GeS_4]$ tetrahedron in L1 and the bowlike $[Sb_2S_6]$ dimer in L2 gives rise to a thick single layer, Figure S3. Then such two thick single layers are further weaved by Ge^{4+} ions resulting in a double-layered $\{Ge_{10}Sb_{28}S_{72}\}^{20-}$ framework. As a result, two types of channels with different shapes are found in compound **1** running along the [1 −1 0] or [1 1 0] directions, Figure 1a. As shown in Figure 1d,e, one is formed by the $[Sb_2S_5]$ dimers interlinking the 18-membered froglike rings with a cross-section of 10.17 × 9.90 Å^2 (Figure 1f), whereas the other is formed by interconnection between the $[Sb_2S_7]$ dimers and the 14-membered crownlike rings with a rough square cross-section of 5.94 × 5.94 Å^2 (Figure 1g).

DOI: 10.1021/acs.inorgchem.5b01181
Inorg. Chem. 2015, 54, 8474−8481

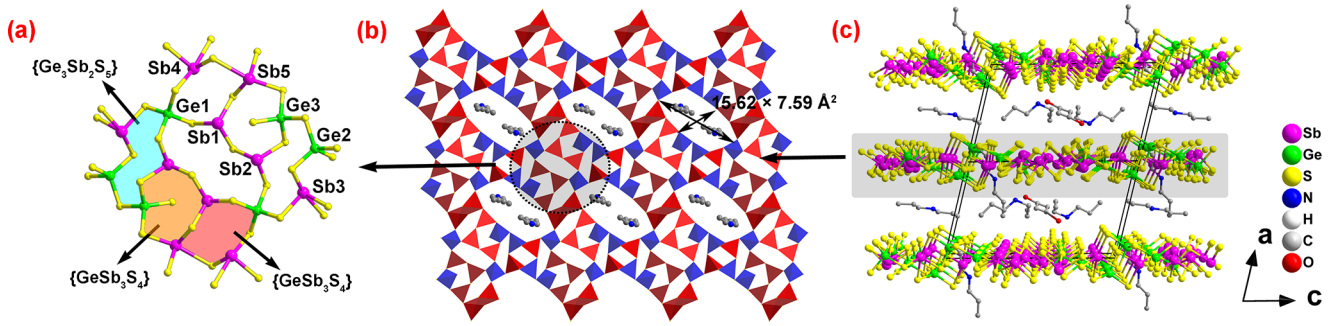

Figure 2. (a) The SBU of compound **2**. (b) Polyhedral view of a $[Ge_3Sb_5S_{15}]^{3-}$ layer in **2** with the $DPAH^+$ cations inserted in the formed windows. (c) Packing diagram of **2** viewed along the *b* axis showing the location of $DPAH^+$ cations and lattice ethanol molecules. H atoms were omitted for clarity.

There exist tetranuclear $\{GeSb_3S_9\}$ and trinuclear $\{GeSb_2S_9\}$ units in compound **1** (Figure S4a,f). Thus far the heterometallic chalcogenido units found in Ge−Sb−S compounds include the trinuclear $\{GeSb_2S_x\}$ (x = 7, 8, 9)[1f,6c,8] (Figure S4d−f), and tetranuclear $\{GeSb_3S_{11}\}$[6i] and $\{Ge_2Sb_2S_7\}$[6c] (Figure S4b,c) units. The trinuclear $\{GeSb_2S_9\}$ unit in compound **1** has been observed in $[(Me)_2NH_2]_2[GeSb_2S_6]$,[1f] while the tetranuclear $\{GeSb_3S_9\}$ unit is formed by one $[GeS_4]$ tetrahedron, one $[SbS_4]$ trigonal bipyramid, and two $[SbS_3]$ pyramids via vertex-sharing, which has never been found in the reported thiogermanate−thioantimonates. The tetranuclear $\{GeSb_3S_9\}$ unit is also different from the reported tetranuclear $\{M_2Sb_2S_9\}$ (M = Ga^{3+}, In^{3+})[7d,13] and $\{M_2Sb_2Q_{10}\}$ (M = In^{3+}, Q = S^{2-}, Se^{2-}; M = Sn^{4+}, Q = S^{2-})[7e,14] units, which are all built with two metal tetrahedra and two asymmetric polyhedra of Sb(III) (Figure S4g,h). Indeed, the backbone of the tetranuclear $\{GeSb_3S_9\}$ cluster might be viewed as an ancestor of the distorted $[In_2Sb_2S_9]$ cluster frequently observed in In−Sb−S compounds,[13] where one $[InS_4]$ tetrahedron of the tetranuclear $\{In_2Sb_2S_9\}$ cluster is replaced by one ψ-$\{SbS_4\}$ trigonal bipyramid.

The methylammonium cations as SDAs and charge-balancing agents along with lattice water molecules are located in the above-described intralayered channels and interlayered spaces, and form extensive N−H···S and C−H···S hydrogen bonds with S atoms of the anionic framework (Figure S5a−c). The N−H···S and C−H···S hydrogen bond distances and angles fall in the range of 3.19(3)−3.60(6) Å and 112.4−176.3°, 3.32(8)−3.78(5) Å and 114.0−173.1°, respectively. After the removal of all the guest molecules and cations in the channels, the effective solvent accessible volume occupies 34.3% of the total cell volume calculated by using the PLATON program.[12]

Crystal Structure Description for Compound 2. Single-crystal X-ray diffraction analysis reveals that compound **2** belongs to the triclinic space group $P\bar{1}$ and features 2D anionic layers parallel to the *bc* plane separated by dipropylammonium cations ($DPAH^+$), Figure 2c. The asymmetric unit of compound **2** contains three crystallographically independent Ge^{4+} ions, five Sb^{3+} ions, 15 S^{2-} ions, three $DPAH^+$ cations, and half an ethanol molecule. All the Ge^{4+} ions are tetrahedrally coordinated by four S atoms with Ge−S bond distances in the range of 2.1679(11)−2.2416(11) Å. Sb(1) and Sb(2) show trigonal pyramid geometries, whereas Sb(3−5) present trigonal bipyramid coordination geometries, in which the Sb−S bond lengths range from 2.4358(10) to 2.5254(10) Å and from 2.4059(11) to 2.9322(12) Å, respectively. The Ge−S and Sb−S bond lengths are comparable to those in the reported Ge−Sb−S compounds.[1f,6c,i,8,9]

Notably there exists a secondary building unit (SBU) with the complex formula of $\{Ge_6Sb_{10}S_{38}\}$ in **2**, Figure 2a. The SBU consists of two identical centrosymmetric parts sharing two Ge1 atoms to form a $\{Ge_2Sb_4S_6\}$ 12-membered ring. Each part contains a $\{Ge_3Sb_2S_5\}$ 10-membered ring formed by corner-sharing of three $[GeS_4]$, one $[SbS_3]$, and one $[SbS_4]$, a $\{GeSb_3S_4\}$ eight-membered ring formed by corner-sharing of one $[SbS_4]$, two $[SbS_3]$, and one $[GeS_4]$, and a $\{GeSb_3S_4\}$ eight-membered ring formed by corner-sharing of two $[SbS_4]$, one $[SbS_3]$, and one $[GeS_4]$. It is worth noting that the SBU of **2** is obviously different from that of $\{In_5Sb_6S_{24}\}$ in 2D-$[(CH_3CH_2CH_2)_2NH_2]_5In_5Sb_6S_{19}\cdot 1.45H_2O$,[6h] Figure S6. The former is composed of four $[SbS_3]$, six $[SbS_4]$, and six $[GeS_4]$, whereas the latter includes six $[SbS_3]$ and five $[InS_4]$.

Each SBU connects to four adjacent SBUs to generate a 2D anionic $[Ge_3Sb_5S_{15}]_n^{3n-}$ layer along the *bc* plane, which is perforated with large elliptical-like windows with a cross-section of 15.62 × 7.59 $Å^2$, Figure 2b. The opening of the window is defined by a 12-membered ring composed of six $[GeS_4]$ tetrahedra, two $[SbS_3]$ trigonal pyramids, and four $[SbS_4]$ trigonal bipyramids by corner/edge sharing, different from that in 2D-$[(CH_3CH_2CH_2)_2NH_2]_5In_5Sb_6S_{19}\cdot 1.45H_2O$,[6h] which is defined by corner-sharing six $[InS_4]$ tetrahedra and six $[SbS_3]$ trigonal pyramids. Then the windows of each layer are aligned with those of neighboring layers, forming channels along the *a* axis that are perpendicular to the layers, Figure 2c.

Hitherto, although several 2D Ge−Sb−S compounds have been synthesized under mild solvothermal conditions using metal complexes (MCs) as SDAs, as exemplified by $[M(en)_3][GeSb_2S_6]$ (M = Mn, Co, Ni, Ge),[6c,8] $[Co(dien)_2]_2GeSb_4S_{10}$,[8a] and $[Ni(dien)_2]_3[Ge_3Sb_8S_{21}]\cdot 0.5H_2O$,[9] no organic amine-directed 2D Ge−Sb−S compounds have been isolated prior to this work. With the exception of compound **1**, compound **2** represents a 2D amine-directed Ge−Sb−S compound based on the complex $\{Ge_6Sb_{10}S_{38}\}$ cluster, which represents a new type of Ge−Sb−S SBU that is quite different than the reported trinuclear $\{GeSb_2S_x\}$ (x = 7, 8, 9)[1f,6c,8] and the tetranuclear $\{Ge_2Sb_2S_7\}$[6c] and $\{GeSb_3S_{11}\}$.[6i]

The $DPAH^+$ cations as SDAs and charge-balancing agents are found in the interlayered spaces and the channels, and they form extensive N−H···S and C−H···S hydrogen bonds with S atoms from the anionic network (Figure S7). The N−H···S and C−H···S hydrogen bond distances and angles fall in the ranges of 3.271(5)−3.683(17) Å and 129.4−176.4° and 3.461(13)−3.789(6) Å and 115.4−169.1°, respectively. The solvent-

DOI: 10.1021/acs.inorgchem.5b01181
Inorg. Chem. 2015, 54, 8474−8481

accessible volume in compound **2** excluding the organic cations is ~55.2% calculated by the PLATON program.[12]

Ion Exchange. The excellent ion-exchange properties exhibited by some porous or layered metal chalcogenides containing organic amine cations[1c−f,6h,15] promoted us to study the ion-exchange property of compound **1**. Our experiments indicated that the kinetics of Cs^+ capture by compound **1** is fast, and the exchange of Cs^+ by compound **1** follows the Langmuir model with a high saturation capacity of 230.91 ± 14.5 mg/g. In particular, compound **1** exhibited the specificity for Cs^+ ion against other cations described in detail as follows. Unfortunately, compound **2** showed no ion-exchange property, despite some similarities with previously mentioned $[(CH_3CH_2CH_2)_2NH_2]_5In_5Sb_6S_{19}\cdot 1.45H_2O$,[6h] where the $[(CH_3CH_2CH_2)_2NH_2]^+$ cations can be partially exchanged by alkali-metal or alkaline earth-metal cations.

Kinetic and Isotherm Studies of Ion Exchange. To gain a comprehensive insight into the Cs^+ ion-exchange performance of compound **1**, the kinetics of Cs^+ ion-exchange was first studied. As presented in Figure 3, the initial concentration of

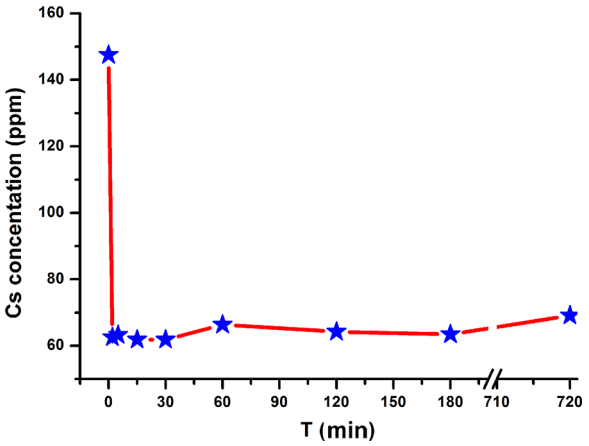

Figure 3. Kinetics of Cs^+ ion-exchange of compound **1** plotted as the Cs^+ ion concentration (ppm) vs the time (min).

Cs^+ decreased steeply and reached the equilibrium within 2 min, indicating an astonishing and extremely rapid kinetic process. The fast removal efficiency is comparable with FJSM-SnS[16] and KMS-1,[1b] and significantly larger than those of the commercial zeolite A[17] and AM-2.[18] This should be attributed to strong interaction between the acidic Cs^+ cations and the S^{2-} ions of the basic framework and to the high mobility of the small organic amines. The small fluctuation of kinetics curve could be attributed to the dynamic Cs^+ ion-exchange process.

To fully characterize the ion-exchange properties of compound **1**, the systematic sorption isotherm study was conducted by varying the concentration of Cs^+ in solution to determine maximum adsorption capacity (q_m). The Cs^+ equilibrium curve is graphed in Figure 4, which is derived from the Cs^+ concentration at equilibrium plotted against the capacity of Cs^+ exchange. Langmuir model could fit the equilibrium isotherm very well with the R^2 = 0.9585. The model is based on the assumptions that the surface containing the equivalent adsorbing sites is homogeneous, the state of the exchanged ions in the structure is definite, the ions on adjacent sites are independent, and each site can catch only one ion.[19] It can be described by eq 1.

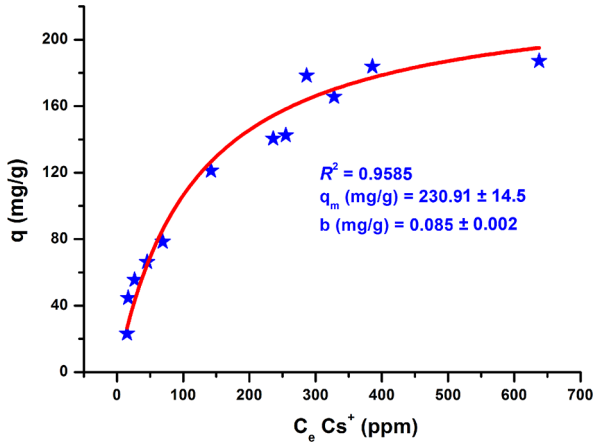

Figure 4. Cs^+ equilibrium curve for compound **1** (pH ≈ 7, V/m = 1000 mL/g, contact time 720 min, at 65 °C, and initial Cs^+ concentrations in the range of 17−825 ppm). The Langmuir equilibrium isotherm is derived from the Cs^+ concentration at equilibrium plotted against the capacity (milligrams of ions removed per gram of sorbent).

$$q = q_{max}\frac{bC_e}{1 + bC_e} \quad (1)$$

Here, C_e (ppm) is the Cs^+ concentration in solution at equilibrium, q (mg/g) is the sorption capacity at equilibrium C_e, q_{max} (mg/g) is the maximum capacity of the sorbent, and b (L/mg) is the Langmuir constant related to the free energy of the adsorption.[19a] The value of q can be calculated from the eq 2.

$$q = \frac{(C_0 - C_f)V}{m} \quad (2)$$

Where C_0 and C_f (ppm) are the initial and equilibrium concentrations, respectively, which could be determined by the AAS method. V (mL) is the volume of the solution and m (g) is the amount of the ion-exchanger used in the experiment.[19a]

The maximum exchange capacity of compound **1** was found to be 230.91 ± 14.5 mg/g, which accounts for 62.6% of the theoretical saturation capacity (484 mg/g) in well agreement with the result of the EDS analysis (Table S2). It is worth noting that the maximum capacity of compound **1** for Cs^+ ion is slightly better than that of KMS-1 (226 mg/g)[1b] and TAM-5 (192 mg/g)[20] and significantly larger than those of commercial AMP-PAN (81 mg/g), which is currently marketed by UOP as IONSIV IE-910.[21]

Competitive and pH-Dependent Ion-Exchange Experiments. Besides the high saturation capacity, compound **1** was notably provided with strong preference for Cs^+ against other alkali or alkaline earth-metal ions, such as Na^+, K^+, Mg^{2+}, and Ca^{2+}. The distribution coefficient K_d was measured. As a measurement of affinity and selectivity, K_d is described as follows:

$$K_d = \frac{V}{m}\frac{(C_0 - C_f)}{C_f} \quad (3)$$

where C_0 and C_f are the initial and equilibrium concentration of M^{n+} (ppm), V is the volume (mL) of the testing solution, and m is the amount of the ion exchanger (g) used in the experiment.[19a]

DOI: 10.1021/acs.inorgchem.5b01181
Inorg. Chem. 2015, 54, 8474−8481

As shown in Figure 5a, the K_d value of Cs^+ for compound **1** is 4.61×10^3 mL/g with the absence of competitive cations, while

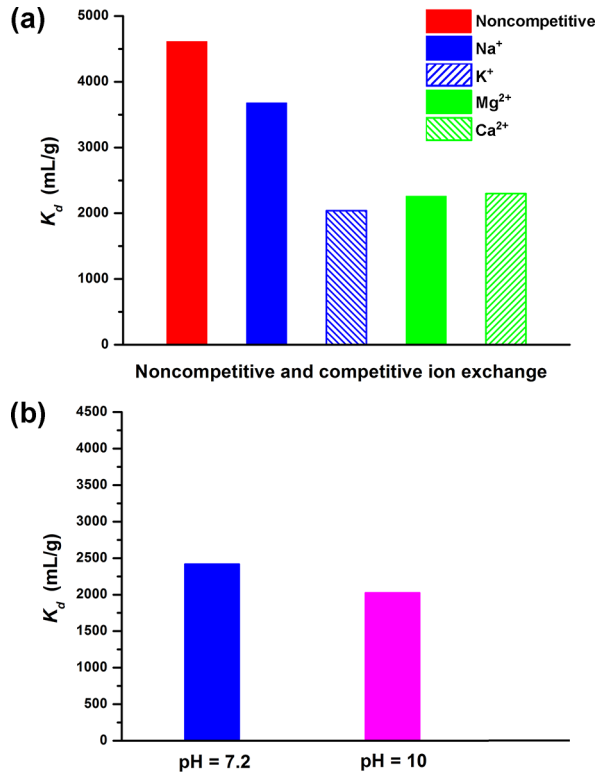

Figure 5. (a) The K_d of Cs^+ in the noncompetitive and individual competitive ion-exchange experiments ($C_0 \approx 9$ ppm, at 65 °C, V/m = 1000 mL/g). (b) The K_d of Cs^+ in the simulated neutral and alkaline groundwater ($C_0 \approx 2$ ppm, at 65 °C, V/m = 1000 mL/g).

the K_d value decreased to 3.68×10^3 mL/g with the presence of ~20-fold excess of Na^+. It is satisfactory for us that the K_d value was still high despite the presence of excess competitive sodium cations. In the case of compound **1** in ~20-fold excess of Ca^{2+}, the affinity and selectivity of compound **1** for Cs^+ is also impressive, with the evidence of the higher K_d value of 2.30×10^3 mL/g. By comparison, KMS-1 was found less than 1×10^2 mL/g with the presence of only 12-fold excess of Ca^{2+}, while the K_d value was more than 1×10^4 mL/g with the absence of competitive cations.[1b] These K_d values revealed that Ca^{2+} was proven to be a stronger competitor than Na^+ for the Cs^+ exchange of compound **1**. Subsequently, the cesium ion-exchange studies in 5 mol/L NaCl solution (neutral pH) were performed because the solutions with high concentration of sodium environment are likely to prevail in realistic nuclear waste. The K_d value presented for Cs^+ in the presence of 5 mol/L NaCl was ~146 mg/L ($C_0 \approx 6$ ppm), which was 8 times higher than that of KMS-2 ($C_0 \approx 6$ ppm).[22] As is known to all, KMS-2 is considered as one of the best and the most potential chalcogenide ion-exchange materials as a Cs^+ scavenger.

In addition, we examined the Cs^+ exchange of compound **1** under the simulated groundwater with pH = 7.2 and pH = 10. In accordance with the expectation, compound **1** still kept the high K_d values, displaying the outstanding preference for Cs^+ ion (Figure 5b). Combined with the above results, obviously compound **1** showed strong preference for Cs^+ ion under competitive conditions. To the best of our knowledge, this "built-in" affinity for Cs^+ of compound **1** is at least partially based on the strong interaction between the acidic Cs^+ cations and the S^{2-} ions of the basic anionic framework, and the appropriate size of channel allowing diffusion of Cs^+ cations.

To fully characterize the ion-exchange properties of compound **1**, investigations were also performed to evaluate the cesium extraction capacity in solutions with different pH. As shown in Figure S8, the exchanged materials could keep crystallinity after immersion in aqueous solutions with different pH. Despite the fact that the crystallinity of plate-like crystals appeared to be poor when the pH was adjusted to 2.8, the structural stability of compound **1** is impressive over such wide pH range (from 2.8 to 11.0), which is very rare in the typical natural mineral ion-exchangers. As shown in Figure 6, the K_d

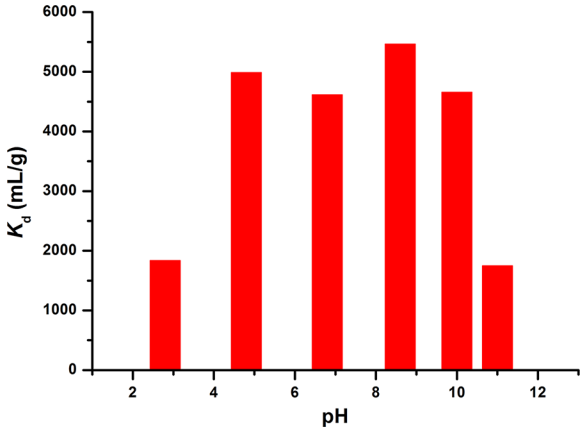

Figure 6. K_d of Cs^+ in individual pH-dependent ion-exchange experiments ($C_0 \approx 9$ ppm, V/m = 1000 mL/g, at 65 °C).

values of compound **1** are 1.84×10^3 at pH = 2.8 and 1.75×10^3 at pH = 11.0. Remarkably, the K_d could reach the value of 5.46×10^3 mL/g at pH = 8.6. This property of compound **1**, combined with its rapid dynamics and high selectivity under competitive conditions, makes it an attractive option for entrapping the Cs^+ from the aqueous solutions.

Despite the significant progress in the search for chalcogenidometalates with great structural and compositional diversities, the research on crystalline chalcogenido ion-exchangers is still in a fledging period. Until now, the exchangeable cations in crystalline chalcogenido ion-exchangers were mainly limited to inorganic cations (typically K^+ ion)[1a,b] and small organic amine cations (typically $CH_3NH_3^+$ and $(Me)_2NH_2^+$ ions;[1c−f] see Table S3). The crystalline chalcogenido ion-exchangers containing larger organic amine cations are still rare.[6h,15] The chalcogenido ion-exchanger with metal-complex cations has not been reported. It is believed that the size difference between the exchangeable cations and the replacing cations and the interactions between the cations and anionic networks somewhat determine whether the ion-exchange process can occur.[1c,e,f] Meanwhile, most of the efficient ion-exchangers have suitable channel size or interlayer spacing, which enable the guest cations to diffuse in and out of the material.[1,6h,15,16] To the best of our knowledge, the supreme selectivity and capacity of compound **1** for specific ions such as Cs^+ may be mainly ascribed to its soft basic framework structure with channels of particular size and shape.[1c,d,f] The lower ion-exchange capacity of **1** for the smaller alkali metal ions, such as Rb^+, K^+, and Na^+, is believed to be due to their larger hydrated spheres.[1e] Such interesting molecule or ion-recognition phenomenon has also been observed in some

DOI: 10.1021/acs.inorgchem.5b01181
Inorg. Chem. 2015, 54, 8474−8481

oxide or chalcogenide materials.[1d,e,23] In contrast to the excellent Cs^+ ion-exchange property of **1**, it is a pity that similar phenomenon has not been found for compound **2**, while the $[(CH_3CH_2CH_2)_2NH_2]^+$ cations in the similar compound $[(CH_3CH_2CH_2)_2NH_2]_5In_5Sb_6S_{19}\cdot 1.45H_2O$[6h] could be partially exchanged by alkali-metal or alkaline earth-metal cations. The differences in the ion-exchange properties between compound **2** and $[(CH_3CH_2CH_2)_2NH_2]_5In_5Sb_6S_{19}\cdot 1.45H_2O$[6h] may originate from the differences in framework composition, size of windows within layer, and hydrogen bonding interactions (Figure S6 and Table S4). The stronger hydrogen bonding interactions in **2** may prevent the guest cations from diffusing in and out of the material. Although here we attempted to make a connection between the structure and ion-exchange properties of known crystalline chalcogenide compounds containing organic amine cations, further in-depth understanding of the ion-exchange mechanism, in particular the correlation of composition, structure, and ion-exchange property, is still in progress, which depends much on a systematical preparation and ion-exchange property studies of the organic-templated chalcogenides.

Optical Properties. The solid-state UV−vis optical absorption spectra of compounds **1**, **2**, and Cs^+-exchanged product of compound **1** are plotted in Figure S16. The optical absorption edges of the above three compounds are estimated to be 2.38, 2.56, and 2.20 eV (Figure 7), respectively, consistent

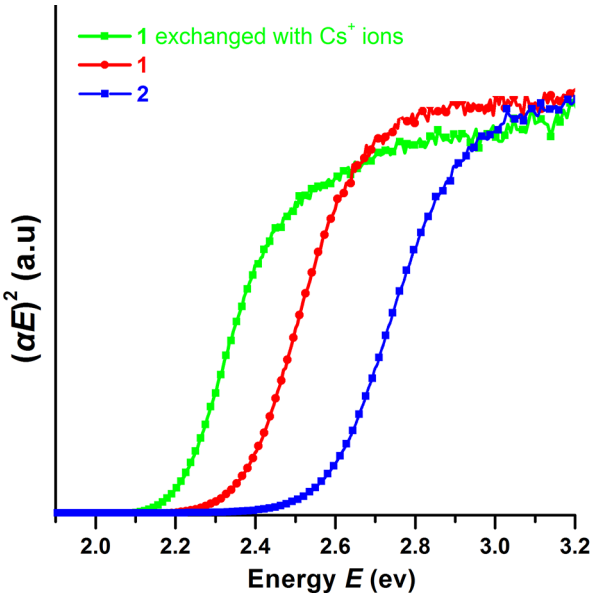

Figure 7. Variation of $(\alpha E)^2$ as a function of photon energy for compounds **1**, **2**, and Cs^+-exchanged product of compound **1**.

with their colors. These absorption edges are compared with the values from other Ge−Sb−S compounds, such as $[(Me)_2NH_2]_2[GeSb_2S_6]$ (2.62 eV),[1f] $[(Me)_2NH_2]_6[(Ge_2Sb_2S_7)(Ge_4S_{10})]$ (2.82 eV),[6c] $[(Me)_2NH_2][DabcoH]_2[Ge_2Sb_3S_{10}]$ (2.64 eV),[6c] $[M(en)_3][GeSb_2S_6]$ (M = Ni (2.05 eV),[6c] Co (2.10 eV),[6c] Ge (2.49 eV),[8b] Mn (2.10 eV)[8a]), $[Co(dien)_2]_2GeSb_4S_{10}$ (2.49 eV).[8b] And it is worth noting that the absorption edge differentiation between pristine compound and Cs^+ ion-exchanged product represents an effective method to tune the band gap of the materials by ion exchange.

Photocatalytic Activity. As a potential and green solution for the global organic contaminants problem, semiconductor photocatalysis technology has received considerable interest due to its better environmental friendliness, suitable operating conditions, and high effectiveness to reduce organic pollutants to lower concentrations. Rhodamine B, which is found to be a highly cytotoxic and refractory fluorescein dye for humans, was selected as a model pollutant to examine the photocatalytic activity of compound **1**. As presented in Figure 8, blank

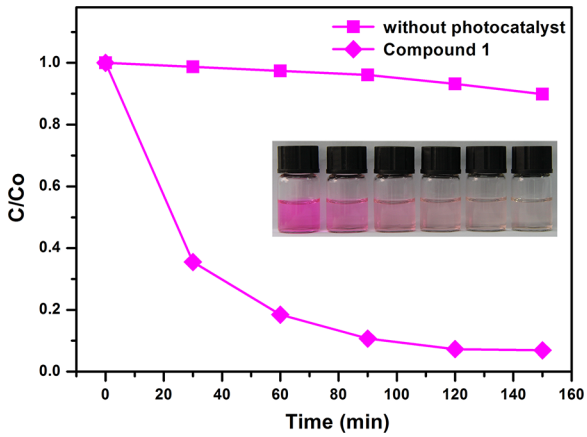

Figure 8. Photodegradation of RhB by compound **1** monitored as the normalized change in concentration as a function of irradiation time.

experiment in the absence of the photocatalyst under visible light irradiation demonstrated that the photolysis of rhodamine B itself was negligible. Satisfyingly, nearly 94% of target contaminant was decolorized after exposure to visible light within 120 min, illustrating an impressive photocatalytic activity of compound **1**. This is in stark contrast with the lengthy degradation time required for other metal chalcogenide photocatalysts, such as $[(Me)_2NH_2]_2In_2Sb_2S_7$,[7e] $[AEPH_2][GeSb_2S_6]\cdot CH_3OH$,[6i] and $[Ni(1,2\text{-dap})_3]HgSb_2S_5$ (1,2-propylene diamine),[6b] which routinely range from 6 h to as much as 8 h. It is worth noting that in addition to high degradation efficiency, compound **1** also kept its better crystallinity, presented in Figure S9. We attribute the high photocatalytic efficiency and high stability to suitable energy band gap corresponding to absorption of visible light compared to various oxide semiconductor materials, coupled with high stability of skeleton structure of metal chalcogenides.

CONCLUSIONS

In summary, two novel amine-directed layered Ge−Sb−S compounds have been solvothermally synthesized and characterized. The double-layered structure of compound **1** is unique and has never been found in layered M−Sb−Q compounds prior to this work, while compound **2** features a unique $[Ge_3Sb_5S_{15}]_n^{3n-}$ slab perforated with large elliptic-like windows. Compound **1** presents an excellent ion-exchanger with particular specificity for Cs^+ ion, and the excellent Cs^+ ion-exchange property can persist in complex competing systems, solutions with high concentration of sodium, and even in both acidic and basic environments. Additionally, compound **1** exhibits excellent visible-light-driven photocatalytic activity for degradation of rhodamine B. Future study will be focused on the exploratory synthesis of Ge−Sb−S functional compounds and deep understanding of relationship between structure and property.

DOI: 10.1021/acs.inorgchem.5b01181
Inorg. Chem. 2015, 54, 8474−8481

■ ASSOCIATED CONTENT

Supporting Information

The Supporting Information is available free of charge on the ACS Publications website at DOI: 10.1021/acs.inorgchem.5b01181. CCDC Nos. 1402150 (**1**) and 1402151 (**2**) contain the supplementary crystallographic data for this paper. The data can be obtained free of charge from The Cambridge Crystallographic Data Centre via www.ccdc.cam.ac.uk/data_request/cif.

Selected bond lengths (tabulated), coordination modes (illustrated), L2 layer, illustrated structural fragment, heterometallic chalcogenido units, packing diagram, powder X-ray diffraction patterns, FT-IR and EDX spectra, EDS and TGA results, and tabulated H-bonding data. (PDF)

X-ray crystallographic information for two compounds. (CIF)

■ AUTHOR INFORMATION

Corresponding Author

*E-mail: xyhuang@fjirsm.ac.cn.

Notes

The authors declare no competing financial interest.

■ ACKNOWLEDGMENTS

This work was supported by the 973 program (No. 2012CB821702), NNSF of China (Nos. 21221001 and 21373223) and Chunmiao project of Haixi institute of Chinese Academy of Sciences (CMZX-2014-001).

■ REFERENCES

(1) (a) Manos, M. J.; Iyer, R. G.; Quarez, E.; Liao, J. H.; Kanatzidis, M. G. *Angew. Chem., Int. Ed.* **2005**, *44*, 3552−3555. (b) Manos, M. J.; Kanatzidis, M. G. *J. Am. Chem. Soc.* **2009**, *131*, 6599−6607. (c) Li, J. R.; Huang, X. Y. *Dalton Trans.* **2011**, *40*, 4387−4390. (d) Wang, K. Y.; Feng, M. L.; Li, J. R.; Huang, X. Y. *J. Mater. Chem. A* **2013**, *1*, 1709−1715. (e) Ding, N.; Kanatzidis, M. G. *Nat. Chem.* **2010**, *2*, 187−191. (f) Feng, M. L.; Kong, D. N.; Xie, Z. L.; Huang, X. Y. *Angew. Chem., Int. Ed.* **2008**, *47*, 8623−8626.

(2) Zheng, N.; Bu, X. H.; Vu, H.; Feng, P. Y. *Angew. Chem., Int. Ed.* **2005**, *44*, 5299−5303.

(3) Zheng, N.; Bu, X.; Feng, P. Y. *Nature* **2003**, *426*, 428−432.

(4) Zhao, L. D.; Lo, S. H.; He, J. Q.; Li, H.; Biswas, K.; Androulakis, J.; Wu, C. I.; Hogan, T. P.; Chung, D. Y.; Dravid, V. P.; Kanatzidis, M. G. *J. Am. Chem. Soc.* **2011**, *133*, 20476−20487.

(5) (a) Xiong, W.-W.; Miao, J.; Ye, K.; Wang, Y.; Liu, B.; Zhang, Q. C. *Angew. Chem., Int. Ed.* **2015**, *54*, 546−550. (b) Xiong, W.-W.; Zhang, Q. C. *Angew. Chem., Int. Ed.* **2015**, DOI: 10.1002/anie.201502277.

(6) (a) Yue, C. Y.; Lei, X. W.; Ma, Y. X.; Sheng, N.; Yang, Y. D.; Liu, G. D.; Zhai, X. R. *Cryst. Growth Des.* **2014**, *14*, 101−109. (b) Yue, C. Y.; Lei, X. W.; Liu, R. Q.; Zhang, H. P.; Zhai, X. R.; Li, W. P.; Zhou, M.; Zhao, Z. F.; Ma, Y. X.; Yang, Y. D. *Cryst. Growth Des.* **2014**, *14*, 2411−2421. (c) Feng, M. L.; Xiong, W. W.; Ye, D.; Li, J. R.; Huang, X. Y. *Chem. - Asian J.* **2010**, *5*, 1817−1823. (d) Spetzler, V.; Näther, C.; Bensch, W. *Inorg. Chem.* **2005**, *44*, 5805−5812. (e) Vaqueiro, P.; Chippindale, A. M.; Cowley, A. R.; Powell, A. V. *Inorg. Chem.* **2003**, *42*, 7846−7851. (f) Wang, K. Y.; Feng, M. L.; Zhou, L. J.; Li, J. R.; Qi, X. H.; Huang, X. Y. *Chem. Commun.* **2014**, *50*, 14960−14963. (g) Feng, M. L.; Li, P. X.; Du, K. Z.; Huang, X. Y. *Eur. J. Inorg. Chem.* **2011**, *2011*, 3881−3885. (h) Ding, N.; Kanatzidis, M. G. *Chem. Mater.* **2007**, *19*, 3867−3869. (i) Feng, M. L.; Hu, C. L.; Wang, K. Y.; Du, C. F.; Huang, X. Y. *CrystEngComm* **2013**, *15*, 5007−5011. (j) Drake, G. W.; Kolis, J. W. *Coord. Chem. Rev.* **1994**, *137*, 131−178.

(7) (a) Kong, D. N.; Xie, Z. L.; Feng, M. L.; Ye, D.; Du, K. Z.; Li, J. R.; Huang, X. Y. *Cryst. Growth Des.* **2010**, *10*, 1364−1372. (b) Wang, K. Y.; Ye, D.; Zhou, L. J.; Feng, M. L.; Huang, X. Y. *Dalton Trans.* **2013**, *42*, 5454−5461. (c) Chen, Z.; Dilks, R. E.; Wang, R. J.; Lu, J. Y.; Li, J. *Chem. Mater.* **1998**, *10*, 3184−3188. (d) Feng, M. L.; Xie, Z. L.; Huang, X. Y. *Inorg. Chem.* **2009**, *48*, 3904−3906. (e) Wang, K. Y.; Feng, M. L.; Kong, D. N.; Liang, S. J.; Wu, L.; Huang, X. Y. *CrystEngComm* **2012**, *14*, 90−94.

(8) (a) Zhou, J.; An, L. T.; Liu, X.; Huang, L. J.; Huang, X. J. *Dalton Trans.* **2011**, *40*, 11419−11424. (b) Powell, A. V.; Mackay, R. *J. Solid State Chem.* **2011**, *184*, 3144−3149.

(9) Zhou, J.; Liu, X.; Liang, G.; Liang, W.; Hu, F.; Zhu, L. *Inorg. Chem. Commun.* **2013**, *27*, 92−96.

(10) (a) Wendlandt, W. M.; Hecht, H. G. *Reflectance Spectroscopy;* Interscience: New York, 1966. (b) Tauc, J.; Grigorovici, R.; Vancu, A. *Phys. Status Solidi B* **1966**, *15*, 627−637.

(11) Sheldrick, G. M. *Acta Crystallogr., Sect. A: Found. Crystallogr.* **2008**, *64*, 112−122.

(12) Spek, A. *Acta Crystallogr., Sect. D: Biol. Crystallogr.* **2009**, *65*, 148−155.

(13) Zhou, J.; An, L.; Zhang, F. *Inorg. Chem.* **2011**, *50*, 415−417.

(14) Feng, M. L.; Ye, D.; Huang, X. Y. *Inorg. Chem.* **2009**, *48*, 8060−8062.

(15) Zhang, R. C.; Yao, H. G.; Ji, S. H.; Liu, M. C.; Ji, M.; An, Y. L. *Chem. Commun.* **2010**, *46*, 4550−4552.

(16) Qi, X. H.; Du, K. Z.; Feng, M. L.; Li, J. R.; Du, C. F.; Zhang, B.; Huang, X. Y. *J. Mater. Chem. A* **2015**, *3*, 5665−5673.

(17) El-Kamash, A. M. *J. Hazard. Mater.* **2008**, *151*, 432−445.

(18) Dobelin, N.; Armbruster, T. *Microporous Mesoporous Mater.* **2007**, *99*, 279−287.

(19) (a) Han, R. P.; Zou, W. H.; Wang, Y.; Zhu, L. *J. Environ. Radioact.* **2007**, *93*, 127−143. (b) Calvet, R. *Environ. Health Persp.* **1989**, *83*, 145−177. (c) Arias, M.; Perez-Novo, C.; Lopez, E.; Soto, B. *Geoderma* **2006**, *133*, 151−159. (d) Do, D. D. In *Adsorption Analysis: Equilibria and Kinetics;* Imperial College Press: London, U.K., 1998; pp 13−17 and 49−57.

(20) Huckman, M. E.; Latheef, I. M.; Anthony, R. G. *Sep. Sci. Technol.* **1999**, *34*, 1145−1166.

(21) Park, Y.; Lee, Y. C.; Shin, W. S.; Choi, S. J. *Chem. Eng. J.* **2010**, *162*, 685−695.

(22) Mertz, J. L.; Fard, Z. H.; Malliakas, C. D.; Manos, M. J.; Kanatzidis, M. G. *Chem. Mater.* **2013**, *25*, 2116−2127.

(23) (a) Johnson, G. M.; Reisner, B. A.; Tripathi, A.; Corbin, D. R.; Toby, B. H.; Parise, J. B. *Chem. Mater.* **1999**, *11*, 2780−2787. (b) Lee, Y. J.; Kim, S. J.; Schoonen, M. A. A.; Parise, J. B. *Chem. Mater.* **2000**, *12*, 1597−1603. (c) Celestian, A. J.; Clearfield, A. *J. Mater. Chem.* **2007**, *17*, 4839−4842. (d) Celestian, A. J.; Kubicki, J. D.; Hanson, J.; Clearfield, A.; Parise, J. B. *J. Am. Chem. Soc.* **2008**, *130*, 11689−11694.

DOI: 10.1021/acs.inorgchem.5b01181
Inorg. Chem. 2015, 54, 8474−8481